

Sandwich-Like Encapsulation of a Highly Luminescent Copper(I) Complex

Marián Matejdes, Matthias Stöter, Rafał Czerwieniec, Markus Leitl, Sabine Rosenfeldt, Thorsten Schumacher, Jonas Albert, Markus Lippitz, Hartmut Yersin,* and Josef Breu*

A small molecular weight cationic copper(I) complex showing high luminescence quantum yield based on a thermally activated delayed fluorescence mechanism is immobilized between two 1 nm thin silicate layers. Partial ion exchange of the emitter into a synthetic layered silicate (fluorohectorite) yields an ordered heterostructure with two types of strictly alternating interlayers: a monolayer of the cationic emitter and a monolayer of hydrated Na⁺ cations. Osmotic swelling of the latter produces dispersions of double-stacks in which the emitter monolayer is encapsulated between two silicate layers. The electrostatic attraction of the emitter interlayer with the oppositely charged silicate layers exerts electrostatic pressure on the emitter. Compared to crystalline salt, rigid confinement for the encapsulated emitter provides improved thermal stability and increased emission quantum yield at ambient temperature. The suspension of delaminated, micrometer-sized double-stacks of 3.9 nm thickness allows for easy solution processing of low-cost optoelectronic devices, such as light-emitting electrochemical cells and organic light-emitting diodes.

subclass of optoelectronic devices generating light from electricity employing electron–hole recombination in an organic semiconductor.

The vacuum processing technique of multilayer optoelectronic devices is compared to solution processing unfavorable due to its high processing costs. Nevertheless, the solution deposition method still suffers from the requirement of orthogonal solvents^[3] due to the possible dissolution of already deposited layers.^[4] Such dissolution processes can result in undesired blending of the different layers causing unwanted decrease of performance. In addition, performance of optoelectronic devices is limited by the diffusion of the emitter molecules.

Thus, improvement of the stability and increase of brightness of optoelectronic devices is highly desirable. One way of addressing this problem is to utilize the crosslinking technique.^[5] For solution-processed optoelectronic devices, this technique enables to prevent the undesired diffusion of the small emitter molecules and results in the enhancement of the structural stability,^[4a,6] improving the device lifetime,^[7] and enhancing the overall performance.^[4b] On the other hand, the achievement of even higher performance can be hampered by the presence of byproducts produced by crosslinking technique.^[8] A recently established method comprising the encapsulation of organic cations and transition metal complexes between negatively charged silicate nanolayers seems to be ideal for these purposes, as the encapsulation is not accompanied by the formation of any unwanted byproducts and at the same time the diffusion of the small emitter molecules is greatly suppressed.^[9] Moreover, this method allows the deposition of active emitter compounds as thin uniform layers with defined thickness. The synthesis approach is based on facile intercalation of the cationic emitter into layered silicate stacks^[9b] forming ordered heterostructures consisting of strictly alternating interlayers occupied with emitter molecules and with inorganic cations (Figure 1b). Similar heterostructures based on synthetic rectorite with alternating nonhydrated potassium and hydrated sodium interlayers were prepared by Möller et al.^[10] In water, these materials undergo osmotic swelling and delaminate into double-stacks of two silicate layers encapsulating the central layer of the intercalated emitter molecules (Figure 1c).^[9c] The double-stacks show very high aspect ratios of more than 5000, with the thickness of the silicate sandwiched


1. Introduction

Nowadays, the global energy market demand has triggered intense research in the development of lighting devices such as the light-emitting electrochemical cell^[1] (LEEC) and organic light-emitting diode^[2] (OLED). LEECs and OLEDs belong to a

Dr. M. Matejdes, Dr. M. Stöter, Dr. S. Rosenfeldt, Prof. J. Breu
Bavarian Polymer Institute and Department of Chemistry
University of Bayreuth
Universitätsstraße 30, D-95447 Bayreuth, Germany
E-mail: Josef.Breu@uni-bayreuth.de

Dr. R. Czerwieniec, Dr. M. Leitl, Prof. H. Yersin
Institute of Physical and Theoretical Chemistry
University of Regensburg
Universitätsstraße 31, D-93053 Regensburg, Germany
E-mail: Hartmut.Yersin@ur.de

Dr. T. Schumacher, Dr. J. Albert, Prof. M. Lippitz
Chair for Experimental Physics III
University of Bayreuth
Universitätsstraße 30, D-95447 Bayreuth, Germany

 The ORCID identification number(s) for the author(s) of this article can be found under <https://doi.org/10.1002/adom.202100516>.

© 2021 The Authors. Advanced Optical Materials published by Wiley-VCH GmbH. This is an open access article under the terms of the Creative Commons Attribution License, which permits use, distribution and reproduction in any medium, provided the original work is properly cited.

DOI: 10.1002/adom.202100516

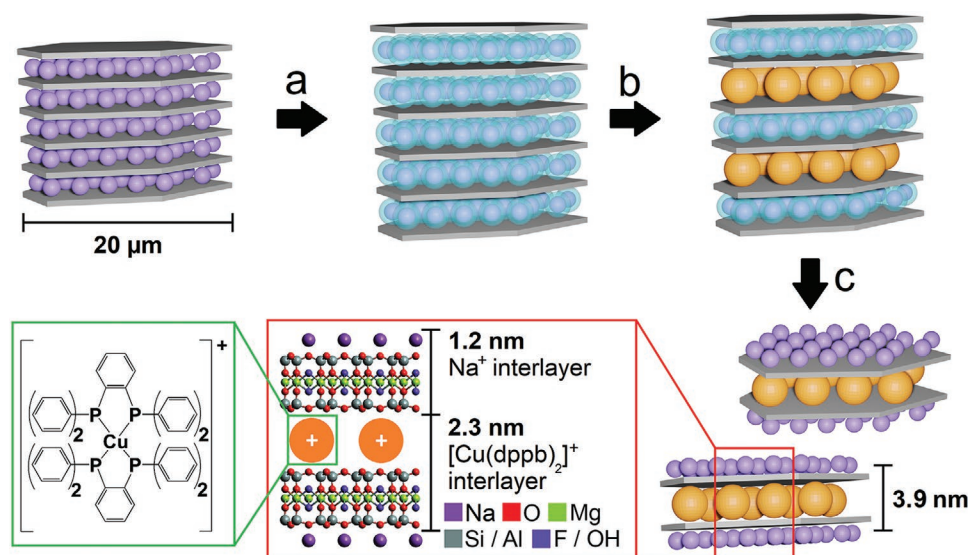


Figure 1. Synthetic procedure for the encapsulation of $[\text{Cu}(\text{dppb})_2]^+$ into Na^+ -hec. a) Crystalline swelling in 75 vol% acetonitrile, b) partial exchange of Na^+ layers by $[\text{Cu}(\text{dppb})_2]^+$ layers with the formation of ordered heterostructures (at a cationic exchange ratio of 22% CEC), and c) complete delamination of double-stacks encapsulating the hydrophobic $[\text{Cu}(\text{dppb})_2]^+$ ions between two silicate layers.

emitter being 3.9 nm and a lateral extension $\approx 20 \mu\text{m}$. Virtually any kind of cationic emitter can be deposited into a device from a solution as a monomolecular layer. In this work, the synthesis of such double-stacks applying sodium fluorohectorite^[11] (Na^+ -hec) and as a representative for such emitters, a luminescent copper(I) complex $[\text{Cu}(\text{dppb})_2]^+$ (dppb = 1,2-bis(diphenylphosphino)benzene, Figure 1)^[12] is demonstrated.

$[\text{Cu}(\text{dppb})_2]^+$ was chosen as a model compound because it is a benchmark cationic copper(I) complex showing thermally activated delayed fluorescence (TADF) at ambient temperature as will be shown below. The advantage of using TADF^[13] materials for lighting applications is based on several aspects. First, they allow for 100% use of singlet and triplet excitons formed in the course of an electroluminescent excitation resulting, according to the singlet harvesting mechanism based on the molecular TADF effect, in very high quantum efficiencies.^[14] Second, concentration quenching or self-quenching at high emitter concentrations, for instance, in crystalline samples, is highly suppressed.^[15] Third, emitters in optoelectronic devices, such as copper compounds, represent an inexpensive alternative for 3rd-row transition metal complexes. Finally, $[\text{Cu}(\text{dppb})_2]^+$ is almost

nonemissive in solvents (see Table 1), and therefore, incorporation into the interlayer space of layered silicate allowed to study the enhancement of photoluminescence by the solid matrix.

2. Results and Discussion

2.1. Ordered Interstratification

The $[\text{Cu}(\text{dppb})_2]^+$ /fluorohectorite sandwich was synthesized according to the procedure illustrated in Figure 1.^[9b,c] As inorganic host synthetic Na^+ -hec with a composition of $[\text{Na}_{0.5}]^{\text{inter}}[\text{Mg}_{2.5}\text{Li}_{0.5}]^{\text{oct}}[\text{Si}_4]^{\text{tet}}\text{O}_{10}\text{F}_2$ was applied, which was prepared by melt synthesis according to a published procedure.^[11] It is transparent and comes in micrometer-sized crystals (Figure S1a, Supporting Information). The cation exchange capacity (CEC) of Na^+ -hec hydrated at 43% relative humidity was determined, applying the $[\text{Cu}(\text{trien})]^{2+}$ method, to be 1.18 mmol g^{-1} .^[9b,16]

For fast kinetics of the intercalation of $[\text{Cu}(\text{dppb})_2]^+$ the one-layer hydrate of Na^+ -hec was first swollen in acetonitrile: water

Table 1. Absorption maxima (λ_{abs}), emission maxima (λ_{em}), photoluminescence quantum yields (ϕ_{PL}), decay times (τ), radiative rates (k^r), and energy gap (ΔE) of $[\text{Cu}(\text{dppb})_2]^+$ as a PF_6^- salt and encapsulated between two silicate layers.

	$[\text{Cu}(\text{dppb})_2](\text{PF}_6)^{\text{a}}$						Encapsulated $[\text{Cu}(\text{dppb})_2]^{\text{b}}$					
	λ_{abs} [nm]	λ_{em} [nm]	ϕ_{PL} [%]	τ [μs]	k^r [s ⁻¹]	$\Delta E(\text{S}_1\text{-T}_1)^{\text{c}}$ [cm ⁻¹]	λ_{abs} [nm]	λ_{em} [nm]	ϕ_{PL} [%]	τ [μs]	k^r [s ⁻¹]	$\Delta E(\text{S}_1\text{-T}_1)^{\text{c}}$ [cm ⁻¹]
THF 300 K	–	550	<1	0.025	–	–	–	–	–	–	–	–
Powder 300 K	279	490	57 ^{d)}	3 ^{d)}	1.9×10^5	800	285	520	65 ^{d)}	7 ^{d,e,f)}	9.3×10^4	435
Powder 77 K	–	510	≈ 100	1900	5.3×10^2	–	–	532	≈ 100	2200 ^{f)}	4.5×10^2	–

^{a)}Compare ref. [12]; ^{b)}Regularly interstratified (alternating heterostructure) sample (22% of CEC; see Table S1, Supporting Information); ^{c)}Energy difference between the lowest excited singlet and triplet states. Roughly estimated from the peak maxima at $T = 300$ and 77 K, respectively; ^{d)}Measured in inert N_2 gas atmosphere. $\lambda_{\text{exc}} = 350 \text{ nm}$; ^{e)}The decay is not monoexponential, reflecting spectroscopic inhomogeneities of the measured material. The value given represents the main (short-lived) component; ^{f)}The decay transients are shown in Figure S4 in the Supporting Information.

mixture (75:25 vol%) (Figure 1a). Swelling in this solvent mixture is limited to the crystalline regime and the basal spacing^[17] expanded in this mixture from $d_{001} = 12.3 \text{ \AA}$ for the one-layer hydrate^[11] to 30.7 \AA for the crystalline swollen Na^+ -hec (Figure S1b, Supporting Information), as determined by means of small-angle X-ray scattering (SAXS). Enlarging the gap opening between adjacent silicate layers to $\approx 21 \text{ \AA}$ (subtracting the layer thickness of hectorite, 10 from 30.7 \AA) facilitates the intercalation of the bulky metal-complex ions $[\text{Cu}(\text{dppb})_2]^+$ of $\approx 10 \text{ \AA}$.

Partial cation exchange leads to segregated dye layers that are arranged in an ordered fashion^[9b,10,18] consisting of strictly alternating hydrated Na^+ and $[\text{Cu}(\text{dppb})_2]^+$ interlayers as evidenced by the appearance of a superstructure reflection (d^{OI}) at a d -spacing of $\approx 35 \text{ \AA}$ (Figure S2, Supporting Information). As previously shown, these ordered heterostructures actually represent the thermodynamic equilibrium.^[9b] The formation of such ordered structures is driven by pronounced differences in interlayer cation densities and different interlayer heights of the hydrated Na^+ and $[\text{Cu}(\text{dppb})_2]^+$ interlayers. To obtain a strictly alternating heterostructure (ordered interstratification), the thrive on forming heterostructures is, however, not yet sufficient. In addition, the probability of the two types of interlayers must be equal. Since the cation densities of the two interlayer types are different, and since the partition function of the dye between intercalated and dissolved state are dependent on the degree of exchange, the concentration of $[\text{Cu}(\text{dppb})_2]^+$ yielding equal probabilities needed to be identified iteratively and was found to be 22% of the total CEC. At this level of partial ion exchange, the intensity of the d_{001}^{OI} at 35.0 \AA was found to be maximal and the series of d_{001}^{OI} reflections was found to be nicely rational with a coefficient of variation of 0.01.

The ideal degree of partial ion exchange was further cross-checked by elemental analysis (Table S1, Supporting Information) and by monitoring the partition equilibria^[9b] in solution (Figure 2). At levels of $[\text{Cu}(\text{dppb})_2]^+$ where the dissolved dye is in equilibrium with the heterostructure, around 54% of the dye remained in solution. To achieve higher levels of dye being ion exchanged, the concentrations need to be significantly higher. At this stage, a new equilibrium is established with 60% of the dye remaining in solution that is in equilibrium with fully exchanged interlayers. The inflection point between the two different equilibria was observed at 22% exchange. Similarly shaped partition functions have been observed with partial ion exchange of Na^+ -hec using other organic cations.^[9b]

Thus, by exchanging 22% of hydrated Na^+ by $[\text{Cu}(\text{dppb})_2]^+$, the two types of interlayers have equal probability and are arranged strictly alternating (Figure 1b) to yield a total composition of $[\text{Na}_{0.39}[\text{Cu}(\text{dppb})_2]_{0.11}][\text{Si}_4[\text{Mg}_{2.5}\text{Li}_{0.5}]\text{O}_{10}\text{F}_2]$ as determined by elemental analysis.

2.2. $[\text{Cu}(\text{dppb})_2]^+$ Encapsulated between Silicate Layers

The alternating heterostructure consists of hydrophobic $[\text{Cu}(\text{dppb})_2]^+$ and hydrophilic Na^+ interlayers. Only the latter are capable to swell osmotically.^[9c,17] When immersing the alternating heterostructure into deionized, pure water, the crystal forceless and spontaneously delaminates into double-stacks,

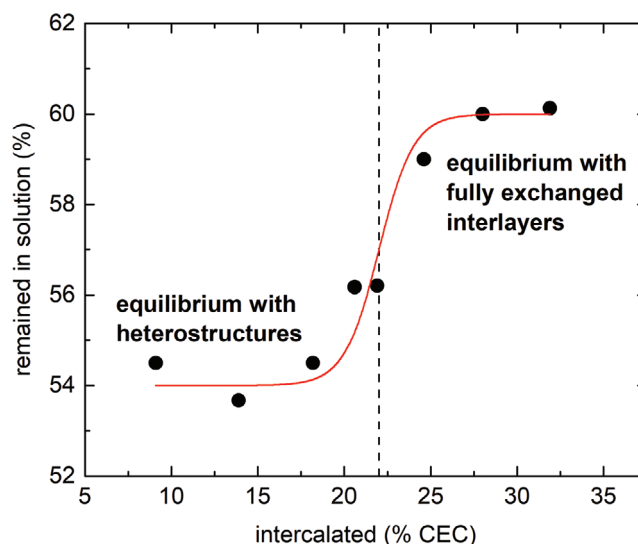


Figure 2. Adsorption isotherm of $[\text{Cu}(\text{dppb})_2]^+$ onto Na^+ -hec in 75 vol% aqueous acetonitrile at $40 \text{ }^\circ\text{C}$ illustrating the transition between the two equilibria at 22% exchange. The red solid line represents a fit to the data points applying an empirical partition function, which is drawn as a guide to the eye. A vertical dashed line indicates the inflection point at which the formation of a perfect, strictly alternating heterostructure occurs with equal probability of the two types of interlayers.

where a hydrophobic monolayer of $[\text{Cu}(\text{dppb})_2]^+$ is encapsulated between the two thin silicate layers (Figure 1c).

The SAXS pattern (Figure 3) for an aqueous 4 wt% suspension of $[\text{Cu}(\text{dppb})_2]^+$ encapsulated between two silicate layers revealed strong form factor oscillations and scatter intensity scaling to q^{-2} typical for platelet-like objects.^[9c] The scatter intensities in the SAXS pattern can be fitted assuming a model of freely rotating double-stacks (see the Experimental section

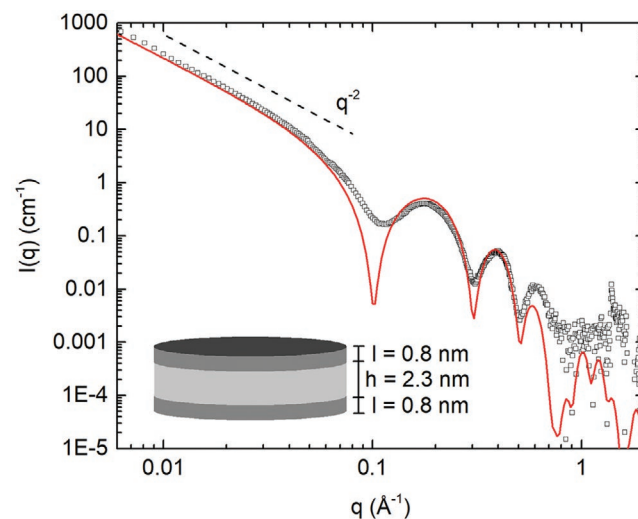


Figure 3. Experimental SAXS patterns (open rectangles) for a 4 wt% aqueous suspension of encapsulated $[\text{Cu}(\text{dppb})_2]^+$ obtained by delamination of partially exchanged Na^+ -hec with the composition of $[\text{Na}_{0.39}[\text{Cu}(\text{dppb})_2]_{0.11}][\text{Si}_4[\text{Mg}_{2.5}\text{Li}_{0.5}]\text{O}_{10}\text{F}_2]$. Solid red line represents calculated scatter intensities for the double-stack model. The dashed line indicates the scatter intensity scaling with q^{-2} typical for platy colloids.

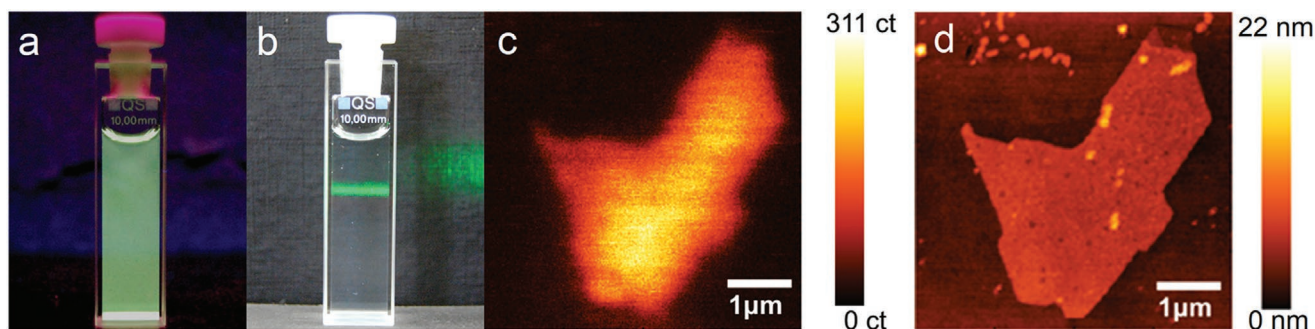


Figure 4. Suspension of encapsulated $[\text{Cu}(\text{dppb})_2]^+$ ($c = 0.5 \text{ mg mL}^{-1}$) in air-equilibrated water a) under UV irradiation at 366 nm and b) in daylight while being illuminated with a green laser pointer. The distinct trace of scattered light proves colloid-sized particles according to the Tyndall effect. c) Photoluminescence map of $[\text{Cu}(\text{dppb})_2]^+$ monolayer encapsulated between the two thin silicate layers with color bar indicating the photoluminescence intensity in counts ($\lambda_{\text{exc}} = 404 \text{ nm}$) and d) AFM height map with corresponding color bar.

for more details) with a total thickness of 3.9 nm, which is in decent agreement with the X-ray data of the heterostructures before delamination. Atomic force microscopy (AFM) images of a dried suspension also confirmed the presence of encapsulated $[\text{Cu}(\text{dppb})_2]^+$ with lateral extensions of several micrometers (Figure S3, Supporting Information) and a thickness of about 4.3 nm, which is again in fair agreement with the SAXS and X-ray results.

2.3. Photophysical and Thermal Properties

The obtained translucent colloidal dispersion showed intense yellow-green luminescence of $[\text{Cu}(\text{dppb})_2]^+$ encapsulated between two silicate layers (Figure 4a,b). The emission is uniformly intense in the whole volume, demonstrating a homogeneous distribution of the encapsulated $[\text{Cu}(\text{dppb})_2]^+$. The proof of the emission originating from the $[\text{Cu}(\text{dppb})_2]^+$ encapsulated between layered silicate platelets was shown by AFM combined with a confocal microscope measurement (Figure 4c,d).

Table 1 compares emission properties of $[\text{Cu}(\text{dppb})_2]\text{PF}_6$ dissolved in tetrahydrofuran (THF), of micrometer-sized powder form, and of a dried powder of $[\text{Cu}(\text{dppb})_2]^+$ encapsulated between two silicate layers. The photoluminescence spectra of the latter are shown in Figure 5. In THF solution, $[\text{Cu}(\text{dppb})_2]\text{PF}_6$ shows only very weak luminescence at 550 nm with the emission quantum yield of $\phi_{\text{PL}} < 1\%$.

The relatively rigid crystalline environment of $[\text{Cu}(\text{dppb})_2]^+$ in the $[\text{Cu}(\text{dppb})_2]\text{PF}_6$ powder reduces vibrational quenching strongly as compared to the solution because molecular distortions in the excited molecules are significantly suppressed leading to an increase of ϕ_{PL} to 57%. At the same time, the emission is blueshifted from 550 nm found for solution to 490 nm for the powder.

Moreover, $[\text{Cu}(\text{dppb})_2]\text{PF}_6$ powder displays distinctly different emission properties at 77 K compared to ambient temperature. In particular, the emission decay times with $\tau(77 \text{ K}) = 1.9 \text{ ms}$ and $\tau(300 \text{ K}) = 3 \mu\text{s}$ differ by orders of magnitude. However, it is more appropriate to compare the radiative rates $k^r = \phi_{\text{PL}}/\tau$ or the radiative decay times. Using the data shown in Table 1, it was found for $T = 77 \text{ K}$ $k^r(T_1 \rightarrow S_1 \text{ phosphorescence}) = 5.3 \times 10^2 \text{ s}^{-1}$ ($\tau = 1.9 \text{ ms}$), representing a relatively

slow decay process compared to other Cu(I) complexes.^[14] For $T = 300 \text{ K}$, the radiative emission rate is determined to $1.9 \times 10^5 \text{ s}^{-1}$ ($\tau = 5.3 \mu\text{s}$). Accordingly, the radiative process is by a factor of almost 360 times faster than at $T = 77 \text{ K}$. This drastic increase is ascribed to the thermal activation process from the T_1 state to the S_1 state combined with a spin-allowed $S_1 \rightarrow S_0$ fluorescence decay path, the TADF emission. Furthermore, it is interesting to obtain an information about the energy gap $\Delta E(S_1 - T_1)$. Frequently, it can be determined from a fitting procedure of the temperature dependence of $\tau(T)$.^[13,14,19] This, however, requires fast thermal equilibration between all states involved. Although this is mostly given for Cu(I) complexes because of very fast intersystem crossing (ISC), being of the order of 10 ps.^[20] As a consequence, also up-ISC (reverse-ISC) is fast and thus, fast equilibration between the lowest excited states results. This leads to a monoexponential decay behavior of the emission. In several cases, however, as found for the compounds investigated, distinct inhomogeneities or even different sites are responsible for the emission. Therefore, decay curves with different decay components occur that are

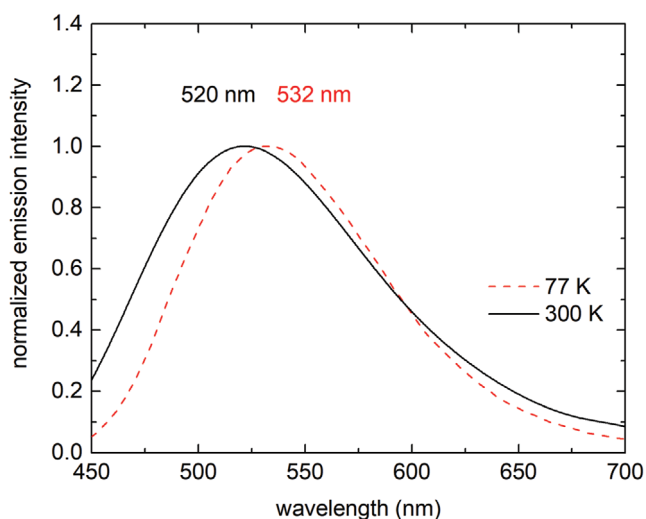


Figure 5. Photoluminescence spectra of a dried powder of $[\text{Cu}(\text{dppb})_2]^+$ encapsulated between two silicate layers at 300 K (black full line) and 77 K (red dashed line) excited at $\lambda_{\text{exc}} = 350 \text{ nm}$.

related to the different sites. In this situation, the fitting procedure is not successful for determining a defined energy gap.^[21] On the other hand, with temperature increase, a blueshift of the emission peak maxima from 510 nm (77 K) to 490 nm (300 K) is observed (Table 1). This shift largely corresponds to the activation energy of this TADF process and therefore, may be taken for a rough estimate of the energy gap. Thus, we find $\Delta E(S_1-T_1) \approx 800 \text{ cm}^{-1}$ ($\approx 100 \text{ meV}$). To summarize, the data presented allow us to safely conclude that the emission behavior for $T > 77 \text{ K}$ becomes dominated by the TADF process up to ambient temperature.

The emission spectra and decay behavior of a dried powder of $[\text{Cu}(\text{dppb})_2]^+$ encapsulated between two silicate layers are comparable to those described for the powder sample of $[\text{Cu}(\text{dppb})_2]\text{PF}_6$, indicating similar electronic structures of the emissive species and similar emission mechanisms. Differences, as marked in Table 1, may be ascribed to the dissimilar environment of the emitting centers. The rigid confinement of the encapsulated $[\text{Cu}(\text{dppb})_2]^+$ also causes a blueshift to $\lambda_{\text{em}} = 520 \text{ nm}$ as compared to the solution of $[\text{Cu}(\text{dppb})_2]\text{PF}_6$ ($\lambda_{\text{em}} = 550 \text{ nm}$). For the encapsulated $[\text{Cu}(\text{dppb})_2]^+$, the quantum yield of $\phi_{\text{pl}}(300 \text{ K}) = 65\%$ was found to be even higher than for $[\text{Cu}(\text{dppb})_2]\text{PF}_6$ powder, indicating that the confinement of $[\text{Cu}(\text{dppb})_2]^+$ encapsulated between oppositely charged silicate layers suppresses nonradiative relaxations to the electronic ground state more efficiently than an ordinary ionic crystalline environment. This correlates well with the longer TADF decay time of $\tau \approx 7 \mu\text{s}$ at ambient temperature, a typical value for Cu(I) complexes.^[14] Importantly, the yellow-green emission was also observed in aqueous suspension of encapsulated $[\text{Cu}(\text{dppb})_2]^+$ (Figure 4).

For completeness, it is remarked that strong emission at a high concentration of the emitter molecules (within the $[\text{Cu}(\text{dppb})_2]^+$ interlayers) is not self-evident. For most Cu(I) complexes flattening distortions^[22] of the molecular structure in the S_1 and T_1 excited states of charge-transfer character results in a loss of resonance condition required for efficient energy transfer between adjacent molecules.^[15c] Therefore, traps of excited Cu(I) complexes are built and consequently concentration quenching or energy transfer to solid-phase defects (quenching traps) are not effective. Obviously, even the electrostatic pressure exerted by the oppositely charged rigid silicate layers does not prevent the important self-trapping effect.^[23] This is in contrast to many conventional emitters, e.g., phosphorescent iridium complexes, where concentration-quenching at higher concentrations is very efficient.^[24]

Interestingly, the encapsulation of $[\text{Cu}(\text{dppb})_2]^+$ between two silicate layers additionally enhances the thermal stability of the complex cation. Thermogravimetric analysis (TGA) revealed thermal stability of the $[\text{Cu}(\text{dppb})_2]\text{PF}_6$ crystals up to 335 °C. Above this temperature, a fast mass loss was observed (Figure S5, Supporting Information). The TGA curve recorded for the encapsulated $[\text{Cu}(\text{dppb})_2]^+$ powder, using the same conditions, displays a mass-loss onset not below 415 °C, thus, pushing the thermal stability by 80 °C. Please note that the initial mass loss commencing at 120 °C is related to the first dehydration step of Na^+ interlayers followed by second dehydration step at 190 °C. Improved stability of the emitter materials applied in optoelectronic devices should enhance their processing and operational stability, resulting in increased device lifetime.

3. Conclusion

In conclusion, highly luminescent layered TADF nanomaterials that may be processed in suspension were synthesized by combining low-cost synthetic silicates and copper(I) complexes. The encapsulation of the TADF emitter improved thermal stability and increased luminescence quantum yields at ambient temperature. The synthesis route involves, in particular, delamination of regularly ordered interstratifications (alternating heterostructures) yielding dispersible double-stacks of densely packed emitter interlayers encapsulated between large and thin transparent silicate layers. The encapsulation immobilizes even low molecular weight emitters, and therefore, this approach enables the application of a myriad of luminescent compounds suitable for optoelectronic devices preventing their diffusion across the device, potentially resulting in enhanced stability, improved device lifetime, and better performance. The presented approach can be extended to diverse osmotically swellable layered inorganic materials, such as zeolites, titanates, niobates, or perovskites,^[25] paving the way to novel nanomaterials for optoelectronic applications with improved quantum efficiencies.

4. Experimental Section

Synthesis of Na^+ -hec and $[\text{Cu}(\text{dppb})_2]\text{PF}_6$: Na^+ -hec with the composition $[\text{Na}_{0.5}]^{\text{inter}}[\text{Mg}_{2.5}\text{Li}_{0.5}]^{\text{oct}}[\text{Si}_4]^{\text{tet}}\text{O}_{10}\text{F}_2$ was synthesized by melt synthesis in a closed molybdenum crucible according to a published procedure.^[26] After the synthesis, the material was annealed for 6 weeks at 1045 °C to improve intracrystalline reactivity, charge homogeneity, and phase purity as described.^[11] $[\text{Cu}(\text{dppb})_2]\text{PF}_6$ was prepared from $[\text{Cu}(\text{CH}_3\text{CN})_4]\text{PF}_6$ and 1,2-bis(diphenylphosphino)-benzene (dppb) according to published procedure.^[12b,27]

Synthesis of $[\text{Cu}(\text{dppb})_2]^+$ Intercalation Compounds: Interstratified samples were prepared in centrifuge tubes sealed with a septum in an Argon atmosphere. Mixing at 40 °C was performed using a temperature-controlled oven equipped with a self-made overhead shaker. During the preparation of intercalated compounds, the amount of solvent was adjusted concomitantly with the variation of the complex amount in order to keep the complex concentration for all samples constant at 1 mmol dm^{-3} . For instance, Na^+ -hec hydrated at 43% relative humidity (10.73 mg) was pre-dispersed in 75 vol% acetonitrile (2.12 cm^3) for 30 min at room temperature using an overhead shaker. After adding of complex solution (4.21 cm^3 in 75 vol% acetonitrile, $c = 1.5 \text{ mmol dm}^{-3}$) the dispersion was mixed at 40 °C for 1 h. The solid was separated by sedimentation followed by centrifugation at $1270 \times g$ for 5 min. The amount of complex remaining in supernatant was determined photometrically using Agilent CARY 300 UV-vis spectrophotometer. The exchanged amount of $[\text{Cu}(\text{dppb})_2]^+$ in intercalated samples was quantified by determining the carbon content using CHN elemental analysis (Elementar vario EL III). Prior to analysis, the samples were thoroughly washed with 75 vol% acetonitrile mixture and two times with pure acetonitrile in order to remove the remaining salts. For weighting, all samples were heated at 110 °C for 2 d and transferred into a glovebox with an argon atmosphere. During the CHN analysis, the combustion temperature was set to 1150 °C using a combustion tube filled with tungsten(VI)-oxide-granules.

After intercalation of $[\text{Cu}(\text{dppb})_2]^+$ the ordered interstratified $[\text{Na}_{0.39}[\text{Cu}(\text{dppb})_2]_{0.11}[\text{Si}_4][\text{Mg}_{2.5}\text{Li}_{0.5}]\text{O}_{10}\text{F}_2$ compound was thoroughly washed three times with a 75 vol% acetonitrile by centrifugation in order to remove the remaining salts. Water was added to the 75 vol% acetonitrile suspension in a dropwise manner up to the point where the concentration of acetonitrile was 25 vol%. Concentration decrease

of acetonitrile results in immediate delamination of the crystalline interstratified material. Acetonitrile was entirely removed by thorough washing with demineralized water followed by centrifugation at $14\,090 \times g$ (Heraeus Multifuge).

Powder X-Ray Diffraction: Diffractograms were recorded in Bragg-Brentano geometry using Panalytical XPERT-PRO diffractometer. Textured films were prepared by drying a few drops of the suspension on microscope slides (Menzel Glass). The glass slides were dried at $80\text{ }^\circ\text{C}$ and equilibrated at room temperature for 12 h at 43% relative humidity (using saturated K_2CO_3 solution).

Small-Angle X-Ray Scattering: A translucent 4 wt% gel in water was prepared by concentrating the aqueous suspension of $[\text{Cu}(\text{dppb})_2]^+$ encapsulated between two silicate layers using a centrifuge (Heraeus Multifuge). Centrifugation was performed two times at $14\,090 \times g$ for 5 min. During the measurement, the gel was placed in a 1 mm glass capillary (Hilgenberg, code 4007610, Germany). SAXS data were obtained by using the Double Ganesha AIR system (SAXSLAB, Denmark). As an X-ray source, a rotating anode (copper, MicoMax 007HF, Rigaku Corporation, Japan) was used, providing a microfocused beam. The data were recorded by a position-sensitive detector (PILATUS 300K, Dectris). In order to cover the range of scattering vectors between 0.004 and 1.3 \AA^{-1} , different detector positions had to be used. Circularly averaged data were normalized to the incident beam, sample thickness, and measurement time prior to the subtraction of the used solvent. The data analysis was performed using the Scatter software (version 2.5), allowing 2D modeling of scattering intensities with respect to the layer distance, mean deviations from the ideal positions, and mean sizes of crystal domains.^[28] Further calculations were done using the SASfit software.^[29]

SAXS Modeling: The SAXS intensities were fitted applying a model of stacked hamburgers.^[9c] For further calculation of the SAXS pattern thickness of 0.8 nm was used for the silicate layer, which was experimentally derived from the intensity minima of the form factor oscillation of completely delaminated Na^+ -hec SAXS patterns. The obtained value is in good agreement with the platelet thickness derived by SAXS measurements of delaminated natural montmorillonites.^[30] The thickness of the $[\text{Cu}(\text{dppb})_2]^+$ layer was found to be 2.3 nm.

Atomic Force Microscopy: The height profile of double-stacks was obtained by using MFP3DTM Atomic Force Microscope (Asylum Research, Santa Barbara, California) equipped with silicon cantilevers (silicon tip, type NSC15/AIBS, Rmash, Tallinn, Estonia). The samples were prepared by dropping a few drops of diluted suspension (0.01 mg dm^{-3}) onto a silicon wafer followed by slow evaporation of water under ambient conditions.

A combination of AFM with luminescence measurements was possible by using a VistaScope AFM (Molecular Vista) equipped with silicon cantilevers (silicon tip ATEC-NC, Nanosensors). The samples for these measurements were prepared by dropping a few drops of diluted suspension (0.01 mg dm^{-3}) onto a glass coverslip followed by slow evaporation of water under ambient conditions. The optical part of the AFM instrument was equipped with a confocal microscope using a UPLSAPO oil immersion lens (Olympus, 100 \times magnification, numerical aperture = 1.4). The sample was excited using a frequency-doubled MIRA Laser source with $\lambda = 404\text{ nm}$ (TiSa—Oscillator, 76 MHz, Coherent). The luminescence was detected by a single-photon avalanche diode (Micro Photon Devices).

Photophysical Characterizations: Photoluminescence spectra were measured with a Horiba Jobin Yvon Fluorolog 3 steady-state fluorescence spectrometer additionally modified, allowing to measure emission decay times. As an excitation source, a PicoQuant LDH-P-C-375 pulsed diode laser ($\lambda_{\text{exc}} = 375\text{ nm}$, full width at half maximum 100 ps) was used. The emission signal was detected with a cooled photomultiplier attached to a FAST ComTec multichannel scalar PCI card with a time resolution of 250 ps. Photoluminescence quantum yields were determined with a Hamamatsu C9920-02 system equipped with a Spectralon integrating sphere.

Thermogravimetric Analysis: To speed up the kinetics of the thermal decomposition, the sample surface was increased by lyophilization

applying a Christ Alpha 1–4 freeze-dryer (Martin Christ). The thermal stability of samples was afterward examined using a thermogravimetric analyzer STA 449 C (Netzsch) in the temperature range of $25\text{--}750\text{ }^\circ\text{C}$ at a heating rate of $10\text{ }^\circ\text{C min}^{-1}$ under a synthetic air atmosphere with a composition of 20.5 vol% O_2 and 79.5 vol% N_2 .

Supporting Information

Supporting Information is available from the Wiley Online Library or from the author.

Acknowledgements

The authors thank Prof. Papastavrou, Physical Chemistry II, University of Bayreuth, for making AFM-equipment available. R.C. thanks the European Research Council (ERC) for support in the framework of the MSCA RISE METCOPH Project 645628. This work was financially supported by the Deutsche Forschungsgemeinschaft (SFB 840).

Open access funding enabled and organized by Projekt DEAL.

Conflict of Interest

The authors declare no conflict of interest.

Data Availability Statement

Research data are not shared.

Keywords

emitter encapsulation, improved emission quantum yield, improved thermal stability, layered silicate, optoelectronic devices, TADF emitters

Received: March 11, 2021

Revised: May 31, 2021

Published online: July 5, 2021

- [1] a) R. D. Costa, E. Ortí, H. J. Bolink, F. Monti, G. Accorsi, N. Armaroli, *Angew. Chem., Int. Ed.* **2012**, *51*, 8178; b) E. Fresta, R. D. Costa, *J. Mater. Chem. C* **2017**, *5*, 5643; c) S. B. Meier, D. Tordera, A. Pertegás, C. Roldán-Carmona, E. Ortí, H. J. Bolink, *Mater. Today* **2014**, *17*, 217.
- [2] a) A. Salehi, X. Fu, D.-H. Shin, F. So, *Adv. Funct. Mater.* **2019**, *29*, 1808803; b) Y. Sun, Y. Jiang, X. W. Sun, S. Zhang, S. Chen, *Chem. Rec.* **2019**, *19*, 1729.
- [3] L. Merklein, M. Mink, D. Kourkoulos, B. Ulber, S. M. Raupp, K. Meerholz, P. Scharfer, W. Schabel, *J. Coat. Technol. Res.* **2019**, *16*, 1643.
- [4] a) D. Volz, T. Baumann, H. Flugge, M. Mydlak, T. Grab, M. Bachle, C. Barner-Kowollik, S. Brase, *J. Mater. Chem.* **2012**, *22*, 20786; b) K. Dey, S. R. Chowdhury, E. Dykstra, A. Koronotov, H. P. Lu, R. Shinar, J. Shinar, P. Anzenbacher, *J. Mater. Chem. C* **2020**, *8*, 11988.
- [5] S. Ho, S. Liu, Y. Chen, F. So, *J. Photonics Energy* **2015**, *5*, 057611.
- [6] N. Ikeda, S. Oda, R. Matsumoto, M. Yoshioka, D. Fukushima, K. Yoshiura, N. Yasuda, T. Hatakeyama, *Adv. Mater.* **2020**, *32*, 2004072.

- [7] a) M. C. Gather, A. Köhnen, A. Falcou, H. Becker, K. Meerholz, *Adv. Funct. Mater.* **2007**, *17*, 191; b) A. Köhnen, N. Riegel, J. H.-W. M. Kremer, H. Lademann, D. C. Müller, K. Meerholz, *Adv. Mater.* **2009**, *21*, 879.
- [8] a) A. Meli, B. Ebenhoch, K. Kutonova, A. Bihlmeier, A. Feyrer, E. Deck, F. Breher, M. Nieger, A. Colsmann, S. Bräse, *Synth. Met.* **2019**, *256*, 116138; b) K. Kutonova, B. Ebenhoch, L. Graf von Reventlow, S. Heißler, L. Rothmann, S. Bräse, A. Colsmann, *J. Mater. Chem. C* **2020**, *8*, 16498.
- [9] a) D. A. Kunz, M. J. Leidl, L. Schade, J. Schmid, B. Bojer, U. T. Schwarz, G. A. Ozin, H. Yersin, J. Breu, *Small* **2015**, *11*, 792; b) M. Stöter, B. Biersack, N. Reimer, M. Herling, N. Stock, R. Schobert, J. Breu, *Chem. Mater.* **2014**, *26*, 5412; c) M. Stöter, B. Biersack, S. Rosenfeldt, M. J. Leidl, H. Kalo, R. Schobert, H. Yersin, G. A. Ozin, S. Förster, J. Breu, *Angew. Chem., Int. Ed.* **2015**, *54*, 4963.
- [10] W. Möller, D. Hirsemann, F. Haarmann, J. Senker, J. Breu, *Chem. Mater.* **2010**, *22*, 186.
- [11] M. Stöter, D. A. Kunz, M. Schmidt, D. Hirsemann, H. Kalo, B. Putz, J. Senker, J. Breu, *Langmuir* **2013**, *29*, 1280.
- [12] a) A. Tsuboyama, K. Kuge, M. Furugori, S. Okada, M. Hoshino, K. Ueno, *Inorg. Chem.* **2007**, *46*, 1992; b) A. Kaeser, O. Moudam, G. Accorsi, I. Séguy, J. Navarro, A. Belbakra, C. Duhayon, N. Armadori, B. Delavaux-Nicot, J. F. Nierengarten, *Eur. J. Inorg. Chem.* **2014**, *2014*, 1345.
- [13] H. Yersin, *Highly Efficient OLEDs: Materials Based on Thermally Activated Delayed Fluorescence*, Wiley-VCH, Weinheim **2019**.
- [14] H. Yersin, R. Czerwieniec, M. Z. Shafikov, A. F. Suleymanova, *ChemPhysChem* **2017**, *18*, 3508.
- [15] a) R. Czerwieniec, J. Yu, H. Yersin, *Inorg. Chem.* **2011**, *50*, 8293; b) R. Czerwieniec, M. J. Leidl, H. H. H. Homeier, H. Yersin, *Coord. Chem. Rev.* **2016**, *325*, 2; c) H. Yersin, A. F. Rausch, R. Czerwieniec, T. Hofbeck, T. Fischer, *Coord. Chem. Rev.* **2011**, *255*, 2622.
- [16] L. Ammann, F. Bergaya, G. Lagaly, *Clay Miner.* **2005**, *40*, 441.
- [17] R. Kunz, S. Amschler, A. Edenharter, L. Mayr, S. Herlitz, S. Rosenfeldt, J. Breu, *Clays Clay Miner.* **2020**, *67*, 481.
- [18] a) W. L. Ijdo, T. Lee, T. J. Pinnavaia, *Adv. Mater.* **1996**, *8*, 79; b) W. L. Ijdo, T. J. Pinnavaia, *J. Solid State Chem.* **1998**, *139*, 281; c) B. L. Sawhney, *Clays Clay Miner.* **1972**, *20*, 93; d) W. L. Ijdo, T. J. Pinnavaia, *Chem. Mater.* **1999**, *11*, 3227.
- [19] a) M. Z. Shafikov, A. F. Suleymanova, R. Czerwieniec, H. Yersin, *Chem. Mater.* **2017**, *29*, 1708; b) H. Yersin, A. F. Rausch, R. Czerwieniec, *Physics of Organic Semiconductors* (Eds: W. Brütting, C. Adachi), Wiley-VCH, Weinheim **2012**.
- [20] a) Z. A. Siddique, Y. Yamamoto, T. Ohno, K. Nozaki, *Inorg. Chem.* **2003**, *42*, 6366; b) H. Yersin, R. Czerwieniec, U. Monkowius, W. M. Kwok, C. Ma, in *ISPPCC Book of Abstracts*, City University of Hong Kong, Hong Kong **2019**, IL-9.
- [21] A. F. Rausch, M. E. Thompson, H. Yersin, *Inorg. Chem.* **2009**, *48*, 1928.
- [22] a) B. Dicke, A. Hoffmann, J. Stanek, M. S. Rampp, B. Grimm-Lebsanft, F. Biebl, D. Rukser, B. Maerz, D. Göries, M. Naumova, M. Biednov, G. Neuber, A. Wetzel, S. M. Hofmann, P. Roedig, A. Meents, J. Bielecki, J. Andreasson, K. R. Beyerlein, H. N. Chapman, C. Bressler, W. Zinth, M. Rübhausen, S. Herres-Pawlis, *Nat. Chem.* **2018**, *10*, 355; b) M. Iwamura, S. Takeuchi, T. Tahara, *Acc. Chem. Res.* **2015**, *48*, 782; c) S. Tschierlei, M. Karnahl, N. Rockstroh, H. Junge, M. Beller, S. Lochbrunner, *ChemPhysChem* **2014**, *15*, 3709.
- [23] a) U. Rössler, H. Yersin, *Phys. Rev. B* **1982**, *26*, 3187; b) G. Gliemann, H. Yersin, *Spectroscopic Properties of the Quasi One-Dimensional Tetracyanoplatinate(II) Compounds*, Springer, Berlin **1985**.
- [24] H. Yersin, *Highly Efficient OLEDs with Phosphorescent Materials* (Ed: H. Yersin), Wiley-VCH, Weinheim, Germany **2008**.
- [25] a) T. Sasaki, M. Watanabe, *J. Am. Chem. Soc.* **1998**, *120*, 4682; b) Y. Ebina, T. Sasaki, M. Watanabe, *Solid State Ionics* **2002**, *151*, 177; c) F. Geng, R. Ma, A. Nakamura, K. Akatsuka, Y. Ebina, Y. Yamauchi, N. Miyamoto, Y. Tateyama, T. Sasaki, *Nat. Commun.* **2013**, *4*, 1632; d) M. Osada, G. Takanashi, B.-W. Li, K. Akatsuka, Y. Ebina, K. Ono, H. Funakubo, K. Takada, T. Sasaki, *Adv. Funct. Mater.* **2011**, *21*, 3482.
- [26] J. Breu, W. Seidl, A. J. Stoll, K. G. Lange, T. U. Probst, *Chem. Mater.* **2001**, *13*, 4213.
- [27] J. R. Black, W. Levason, M. D. Spicer, M. Webster, *J. Chem. Soc. Dalton Trans.* **1993**, *20*, 3129.
- [28] S. Förster, S. Fischer, K. Zielske, C. Schellbach, M. Sztucki, P. Lindner, J. Perlich, *Adv. Colloid Interface Sci.* **2011**, *163*, 53.
- [29] I. Bressler, J. Kohlbrecher, A. F. Thunemann, *J. Appl. Crystallogr.* **2015**, *48*, 1587.
- [30] E. Paineau, I. Bihannic, C. Baravian, A.-M. Philippe, P. Davidson, P. Levitz, S. S. Funari, C. Rochas, L. J. Michot, *Langmuir* **2011**, *27*, 5562.